Journal of Crystal Growth 311 (2009) 3989–3996

Contents lists available at ScienceDirect

Journal of Crystal Growth

journal homepage: www.elsevier.com/locate/jcrysgro

Synthesis, characterization and optical properties of ZnO nanoparticles with controlled size and morphology

Amel Dakhlaoui [b,c,*], Mouna Jendoubi [a], Leila Samia Smiri [a], Andrei Kanaev [d], Noureddine Jouini [b]

[a] Unité de recherche 99/UR12-30, Département de Chimie, Faculté des Sciences de Bizerte 7021 Jarzouna, Tunisie
[b] Laboratoire des Propriétés Mécaniques et Thermodynamiques des Matériaux, LPMTM, CNRS UPR 9001 Université Paris XIII, 99 Avenue J.B. Clément, 93430 Villetaneuse, France
[c] Laboratoire de Physique et Chimie des Nano-Objets, INSA de Toulouse, 135 Avenue de Rangueil 31077 Toulouse cedex 4, France
[d] Laboratoire d'Ingénierie des Matériaux et des Hautes Pressions—LIMHP, CNRS, Institut Galilée, Université Paris 13, 93430 Villetaneuse, France

ARTICLE INFO

Article history:
Received 22 January 2009
Received in revised form
8 June 2009
Accepted 12 June 2009
Communicated by H. Fujioka
Available online 21 June 2009

PACS:
81.05.Dz
81.10.Dn
78.67.–n
78.67.Bf

Keywords:
A1. Crystal growth
A2. Polyol forced hydrolysis
B1. Zinc oxide
B2. Luminescence

ABSTRACT

Zinc oxide monodispersed nanoparticles were synthesized using a modified polyol process without any requirement to use a catalyst or calcination step at high temperature. The morphology and the size of the resulting oxide particles were adjusted by using several synthesis parameters (temperature, alkaline ratio, hydrolysis ratio, etc.). The increasing of the alkaline ratio results in a great change of the elaborated particles morphology that evolved from irregular and anisotropic forms (conical, nanorod-like and elliptical) to spherical one. A growth mechanism of these particles was proposed on the basis of zincite crystal structure and the morphology evolution as a function of the synthesis parameters. The photoluminescence spectra show UV-excitonic and visible emission bands. The strongest intensity of the visible emission was observed in nanorod-like particles, which implies an increased fraction of oxygen vacancies in this sample. The rod-like particles with 1 μm length show the dominant UV-emission, which evidences their improved stoichiometry.

1. Introduction

Zinc oxide is one of the most important semi-conductor materials with tremendous scientific and technological interest. ZnO nanoparticles have been widely used in many industrial areas such as solar cells, UV light-emitting devices, gas sensors, photocatalysts, pharmaceutical and cosmetic industries [1–5]. However, to obtain this oxide with interesting properties and for the development of novel devices, the structure and the microstructure (surface quality, the shape and the size, etc.) of the elaborated particles should be highly controlled. Several physical and chemical methods have been developed to obtain these starting nanocrystals: the solid state reaction [6], chemical vapor transport (CVT) [7], mechanochemical processing [8], vapor phase oxidation of Zn powders [9], hydrothermal process [10], sol–gel process [11] and forced hydrolysis in polyol medium [12–16]. The prepared particles exhibit diverse morphologies (spheres, plates, rod-like, belt, wires, flowers-like, shuttles-like, worms-like, tetrapod, etc.). Nevertheless, most of the physical methods used required high temperatures and expensive equipment, and a lot of the chemical methods necessitate rigorous manipulation of the reaction conditions and high-temperature calcinations to obtain well-crystallized particles, which may limit the application of this material. The synthesis using the polyol process permits the elaboration of ZnO with a narrow size distribution, a controlled morphology and high crystalline quality. It consists in precipitating the oxide particles within the polyol solvent starting from a zinc salt. Its peculiarity lies in the role played by the polyol as a solvent, as a complexant agent and as a surfactant agent which adsorbs on the surface of the elementary particles preventing their agglomeration. Moreover, the high dielectric constant of the polyol liquid lets dissolve a lot of inorganic salts. Its high boiling temperature allows reactions to be conducted in a wide domain of temperature up to 245 °C for the diethylene glycol (DEG). Using this synthesis process, Jézéquel et al. [13] and Poul et al. [14, 15] have elaborated micrometric and sub-micrometric ZnO particles with a relatively controlled shape and size by hydrolysis of zinc acetate dihydrate in diethylene glycol with a heating temperature

* Corresponding author at: Laboratoire des Propriétés Mécaniques et Thermodynamiques des Matériaux, LPMTM, CNRS UPR 9001 Université Paris XIII, 99 Avenue J.B. Clément, 93430 Villetaneuse, France. Tel.: +33 149403496; fax: +33 149403938.
E-mail address: dakhlaoui_amel@yahoo.fr (A. Dakhlaoui).

0022-0248/$ - see front matter © 2009 Published by Elsevier B.V.
doi:10.1016/j.jcrysgro.2009.06.028

ranging from 100 to 220 °C. Particle size has been discussed as a function of the hydrolysis ratio. Recently, Lee et al. [16] have succeeded in synthesizing ZnO particles in polyol medium starting from zinc acetate dihydrate and the polyvinylpyrrolidone (PVP). They discussed the variation of the particles morphology as function of the amount of water and the method of its addition to the reaction medium. In our study, we have prepared ZnO nanoparticles with different morphologies, excellent crystallinity, special dispersion and good reproducibility by adjusting different synthesis parameters. A growth mechanism of the ZnO particles was proposed on the basis of the evolution of the morphology of the elaborated particles in relation to the concentration of the OH^- ions. The optical properties of the as-synthesized particles have been investigated in relation to their morphologies and in regard to high-resolution transmission microscopy results and UV–vis and photoluminescence (PL) measurements.

2. Synthesis and characterization

To synthesize the ZnO nanoparticles, zinc acetate dihydrate ($Zn(OAc)_2.2H_2O$) (4 g), sodium hydroxide (NaOH) (0–8 g) or sodium acetate trihydrate ($Na(OAc).3H_2O$) (13.61 g) and appropriate amount of distilled water were successively dissolved in 50 ml of polyol (diethylene glycol, ethylene glycol (EG) or 1, 2-propanediol (PEG)) and then heated at the desired temperature for 4 h under continuous mechanical agitation. At the end of the reaction, the precipitate was centrifuged, washed several times with ethanol and acetone, and then dried in vacuum at 50 °C.

X-ray patterns of the powders were recorded using an INEL diffractometer with a cobalt anticathode ($\lambda = 1.7890$ Å). The crystallite sizes have been calculated using the Scherrer's relation $L = 0.94\lambda/\beta\cos\theta$, where λ is the wavelength of the X-ray radiation, θ the brag angle of the corresponding peak and β the angular width of the peak at half of its maximum intensity (full-width at half-maximum (FWHM)). The size and the shape of the particles were determined using a JEOL 2011 high resolution transmission electron microscope (HRTEM) and a LEICH 440 scanning electron microscope (SEM). Thermo-gravimetric (TG) measurements were recorded on a SETSYS Evolution-1750 SETARAM instrument under Ar atmosphere and with a heating rate of 10 K min^{-1}. The IR data were collected in the 4000–1000 cm^{-1} range with a Perkin-Elmer FT-IR Spectrum BX spectrophotometer using the KBr pellet technique. The UV–vis spectra were recorded on a Cary 56E spectrophotometer equipped with a PTFE-coated integration sphere. The PL measurements were carried out at room-temperature (RT) using a Nd:Yag (3rd harmonics, 355 nm, 5 ns) laser as the light source with a fluence of 2.0 mJ/cm^2 on the sample. An intensified CCD camera by Princeton Instruments coupled to the monochromator Chromex (grating 150 l/mm, $f = 30$ cm, slit 20 μm) were used for the spectra accumulation. A time-window of 100 ns was employed after the laser pulse to avoid contamination of measured PL spectra by the scattered laser light.

3. Results and discussion

Several synthesis parameters such as the temperature of the reaction, the nature of the solvent, the hydrolysis ratio ($h = n_{water}/n_{metal}$) and the basic ratio ($b = n_{sodium\ hydroxide}/n_{metal}$) have been varied in this study resulting in particles with different sizes and shapes (cone, nanorods, spheres and rods) as summarized in Table 1.

The XRD patterns of all the as-synthesized powders revealed well-crystallized and pure ZnO particles with the hexagonal würtzite phase (space group $P6_3mc$, JCPDS 36-1451) (Fig. 1). The measured lattice constants a and c were 3.249(2) and 5.208(3) Å ($c/a = 1.603$), respectively. Comparison of all the diffraction patterns revealed only a slight variation of the (0 0 2) peak's intensity as a function of the particles morphologies (spheres, nanorods, cones and rods) indicating different orientation growth of the ZnO particles. The crystallite sizes (Table 2), estimated from the FWHM of the (1 0 0), (0 0 2) and (1 0 1) diffraction peaks show

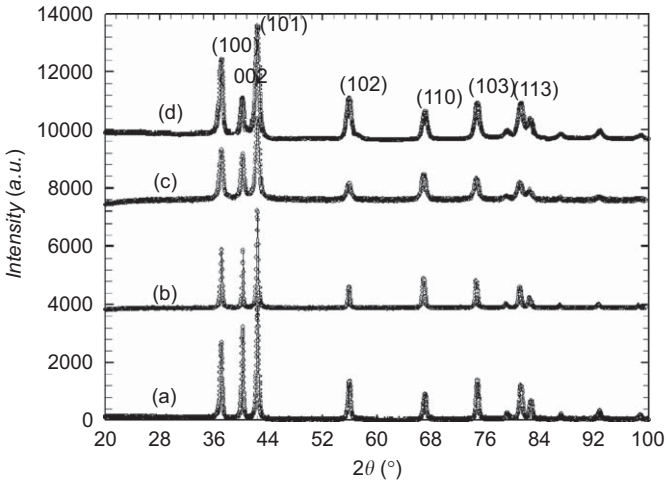

Fig. 1. Powder X-ray diffraction patterns of the as-synthesized ZnO (a) conical particles, (b) nanorods, (c) spherical particles and (d) rod-like particles.

Table 1
The most attractive results obtained as a function of different synthesis conditions.

Sample	[Zn]	$b = n_{sodium\ hydroxide}/n_{metal}$	$h = n_{water}/n_{metal}$	Temperature (°C)	Solvent	Morphology of the powder
Zn_{20}	0.5	2	20	100	DEG	Irregular
Zn_{21}	0.5	2	20	180	DEG	Elliptical
Zn_{22}	0.5	2	20	245	DEG	Nanorods
Zn_{23}	0.5	2	20	198	EG	Elliptical
Zn_{24}	0.5	2	20	185	PEG	Elliptical
Zn_{25}	0.5	0	20	245	DEG	Mostly conical shape
Zn_{26}	0.5	0.5	20	245	DEG	Conical
Zn_{27}	0.5	1	20	245	DEG	Conical
Zn_{28}	0.5	1.5	20	245	DEG	Conical+hexagonal plates
Zn_{29}	0.5	3	20	245	DEG	Elliptical+little amount of nanorods
Zn_{30}	0.5	4	20	245	DEG	Spherical
Zn_{30acet}	0.5	4 (Sodium acetate)	20	245	DEG	Rod-like

Table 2
As-elaborated particle size, estimated crystallite size, measured intensity ratio of the PL emission bands in the ultraviolet and visible regions and bandgap.

Sample	Dimensions of the particles		Crystallite size calculated from the peaks			I_{UV}/I_{Vis}	Eg (eV)
			(1 0 0)	(0 0 2)	(1 0 1)		
Zn_{22}	33–50	100–200	33	54	32	0.49	3.25
Zn_{28}	60	100–250	29.7	41	28.7	3.22	3.27
Zn_{30}	20–30		16.5	19.4	17.4	0.9	3.25
Zn_{30Ac}	80	1000	53.4	65.8	53.7	8.33	3.28
Zn_{23}	25–35		21.3	18.7	20.6	5	3.19

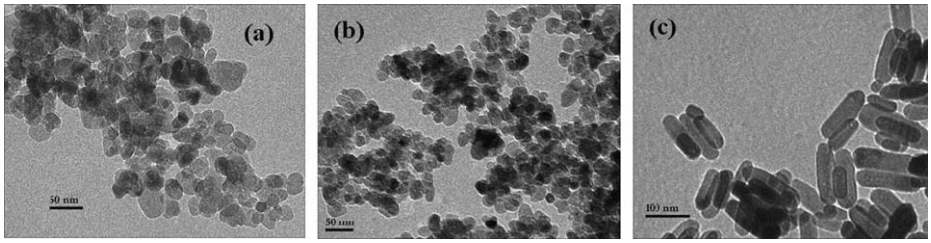

Fig. 2. Transmission electron microscopy images of ZnO nanoparticles grown at 100 °C (a) 180 °C (b) and 245 °C (c).

a slight increase of the dimension of the crystallites along the *c*-direction for particles with conical and nanorods-like morphologies as well as for the rod-shaped particles which confirms their orientation growth along this axis.

3.1. Effect of the reaction temperature

Reactions have been performed at different temperatures fixing the other synthesis parameters (solvent = DEG, $h = 20$, $b = 2$, $[Zn(OAc)_2\cdots 2H_2O] = 0.5$ M and $t = 4$ h). Transmission electron microscope (TEM) micrographs of the obtained ZnO particles show a clear difference between samples Zn_{20}, Zn_{21} and Zn_{22} prepared at 100, 180 and 245 °C, respectively; particles elaborated at 100 °C have nanometric size but no regular shape (Fig. 2a). The morphology and the size distribution were clearly improved when the temperature was increased up to 180 °C (Fig. 2b); the particles become almost regular with elliptical shape and with a size in the range 20–40 nm. When the mixture was heated at the boiling temperature of the solvent (245 °C), nanorods with 33–50 nm in diameter and 100–200 nm in length were obtained (Fig. 2c). TEM images of the latest particles realized at different tilt positions of the grid ($x = 0$, 20 and 33) (Fig. 3) were almost the same, which confirms their nanorod-like morphology.

To study the effect of the other synthesis parameters on the particles morphology, the reactant mixture is heated to the boiling temperature of the solvent.

3.2. Effect of the solvent

Synthesis parameters were fixed to the same as those of the sample Zn_{22} replacing the diethylene glycol by ethylene glycol (EG) (sample Zn_{23}) and 1, 2-propanediol (sample Zn_{24}), respectively. In these two latest solvents, particles present almost the same elliptical morphology which differs from that of particles obtained in the DEG (sample Zn_{22}). This difference could be related not to the nature of the solvents itself but to their boiling temperatures, (198 °C for EG and 185 °C for PEG) that are lower than that of the DEG. In fact, when studying the effect of temperature of the reaction medium in DEG, we have noted that for a moderated temperature of 180 °C particles present an elliptical morphology (sample Zn_{21}) close to that obtained in EG and PEG.

3.3. Effect of the hydrolysis ratio

The effect of the hydrolysis ratio *h* on the particles morphology has been earlier studied [14,16]. It has been reported that an increase of *h* leads to an increase of particle size with a slight variation of the morphology. The results obtained here point out those obtained by Poul et al. [14] and Lee et al. [16] with a slight modification due to the addition of sodium hydroxide in our case; for the medium hydrolysis ratio the particles obtained were nanometric with different morphologies and when the hydrolysis ratio increases, they begin to agglomerate and lose their regular shape.

3.4. Effect of the alkaline ratio and growth mechanism

In order to statistically identify the role of the concentration of OH^- ions in determining the morphology of the synthesized ZnO particles, the alkaline ratio *b* has been varied from 0 to 8 while fixing the other synthesis parameters identical to those of the sample Zn_{22} (solvent = DEG, $h = 20$, $[Zn(OAc)_2\cdots 2H_2O] = 0.5$ M and $t = 4$ h). ZnO particles with mostly conical shape were obtained when the alkaline ratio was fixed to zero (sample Zn_{25}) (Fig. 4a). At the alkaline ratio of 0.5 and 1 (samples Zn_{26} and Zn_{27}), the elaborated particles present a conical morphology (Fig. 4b). A mixture of hexagonal plates and particles with conical morphology were obtained when the alkaline ratio was elevated to 1.5 (sample Zn_{28}, Fig. 4c). At alkaline ratio of 2, homogeneous nanorods were obtained (sample Zn_{22}, Figs. 2c and 4d). Selected area electron diffraction (SEAD) pattern on one nanorod (the inset of Fig. 4d) reveals its single crystalline structure and its growth along the *c*-axis. Furthermore, the spacing between diffraction spots developed in the great axis of the nanorods gives a value of 0.26 nm which corresponds to *d* spacing of the (0 0 2) planes, confirming that the cones and the nanorods are oriented in the *c*-direction. This growth habit of ZnO particles along the *c*-direction is in good agreement with the results of several previous reports [17–21]. By increasing the alkaline ratio, the

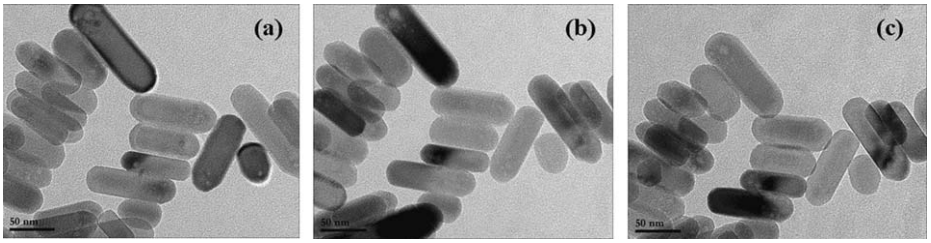

Fig. 3. Transmission electron microscopy micrographs of the ZnO nanorods obtained at different tilt positions (a) $x = 0$, (b) $x = 20$ and (c) $x = 30$.

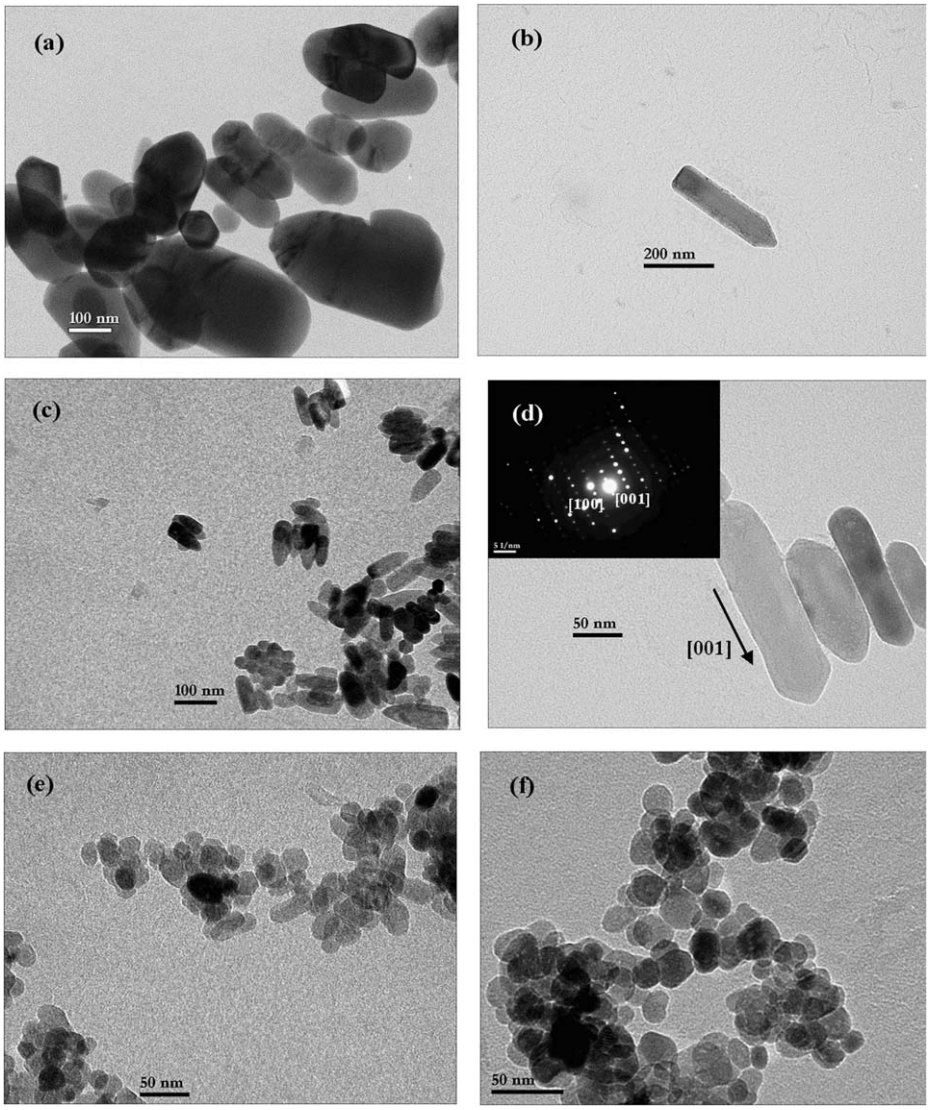

Fig. 4. TEM micrographs of ZnO nanopowder obtained at different alkaline ratios (a) $b = 0$, (b) $b = 0.5$, (c) $b = 1.5$ and (d) $b = 2$, within inset the SAED pattern on one nanorod, (e) $b = 3$, (f) $b = 4$.

stretched growth along the *c*-axis of the ZnO particles seems to be inhibited; the elaborated particles present an elliptical morphology with very little amount of nanorods (sample Zn_{29}, Fig. 4e) when the alkaline ratio is fixed to three and then a spherical morphology when the alkaline ratio is increased up to four (sample Zn_{30}, Fig. 4f). This latest morphology was conserved for alkaline ratios greater than four, i.e. 6 and 8. The preparation Zn_{30acet} was synthesized in the same experimental conditions as those of the Zn_{30} with sodium acetate trihydrate instead of sodium hydroxide. A surprising and drastic change of the particles morphology was observed; it evolves from spherical to rod-like with 80 nm in diameter and 1 μm in length (Fig. 5).

At a first sight, the variation of the ZnO particles morphology as a function of the concentration of $[OH]^-$ ions could be explained as follows: after nucleation and when the crystallite size reaches a critical value of few nanometers (Table 2), the polyol molecules that are non-polar species adsorb on the non-polar planes of the crystallites, thus avoiding the growth perpendicular to these faces resulting in 20–30 nm in diameter monocrystalline primary particles (Fig. 6). The presence of solvent molecules on the

surfaces of the particles was supported by Fourier transform-infrared (FT-IR) spectroscopy (Fig. 7). Indeed, the main bands present in the spectrum of ZnO powder are characteristic of diethylene glycol. The evolution of the morphology of these primary particles depends on the OH^- concentration; for a weak concentration ($b = 0$–1.5), no significant effect on the growth velocity of the various crystal planes was observed; the polar positive face (0 0 1) was the faster to be developed resulting in the ideal conical morphology of the ZnO particles (Fig. 8a). When the concentration of OH^- ions is slightly elevated ($b = 2$), the two polar faces (0 0 1) and (0 0 $\bar{1}$) grew at approximately the same velocity resulting in a nanorod-like morphology (Fig. 8b). Finally, when the OH^- concentration further increased ($b > 3$), a large quantity of OH^- ions adsorbed on the polar faces impeding the growth according to the *c*-direction resulting in particles of elliptical shape (Fig. 8c). For even higher OH^- concentration, no preferential growth along the *c*-axis was observed and the primary particles retained their spherical morphology and nanometric size (Fig. 8d). Wang et al. [22] have also observed the influence of the additive OH^- on the ZnO particles morphology; they noted that in neutral or weak alkalinity solution, the particles appear in elongated cone form. In solution of moderate alkalinity, the particles are short large cone-shaped (the aspect ratios (length/width) decrease) and finally for an elevated alkalinity solution the particles appear in spherical shape and have the regular polyhedral faces. The tendency of the morphological change of ZnO crystallites noted by Wang et al. is close to that observed here; for a weak or elevated amount of additive OH^- ions, the particles morphology is the same. This group had not observed the nanorods and the elliptical morphologies for intermediate amount of additive OH^- ions but had observed a conical form with larger diameter. This difference is introduced by the reaction medium, especially by the solvent used in the two cases. In our case, the presence of the polyol molecules adsorbed on the non-polar faces of the crystallites prevents their growth and the only crystal planes that are able to develop are the two polar faces so that we obtained the nanorods for a medium amount of additive OH^- ions and the elliptical when the OH^- concentration is slightly increased. In the case of the work by Wang et al., the absence of molecules adsorbed on the non-polar faces let them develop faster than the negative polar face leading to the short large conical shape.

On the basis of these observations and previous results [14,23–25], a plausible growth mechanism of ZnO particles could be represented as follows:

(i) firstly the zinc acetate dihydrate gradually dissolves in the DEG, the water molecules and the acetate anions were thus partially replaced by the diethylene glycol units through the formation of Zn–OH and Zn–O coordination bonds to give an intermediate precursor supposed to be an alkoxyacetate complex with the general formula $Zn(OAc)_{2-x}(O(CH_2)_2O(CH_2)_2O)_x$. The formation of the coordination bonds between the metallic cations and the solvent has been clearly evidenced in several previous works [14,23–25]. Indeed Poul et al. [23,24] have already isolated and characterized two

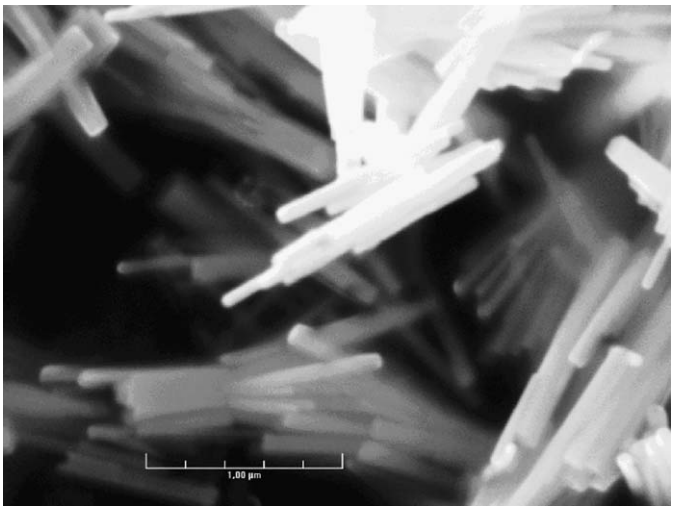

Fig. 5. SEM micrograph of the Zn_{30acet} powder.

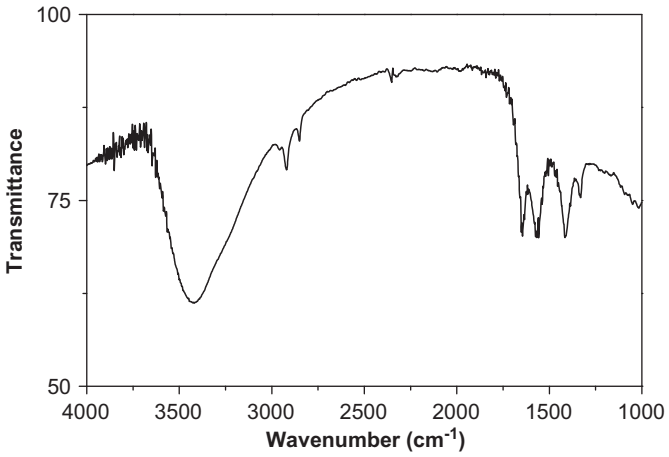

Fig. 7. IR spectrum of the conical particles.

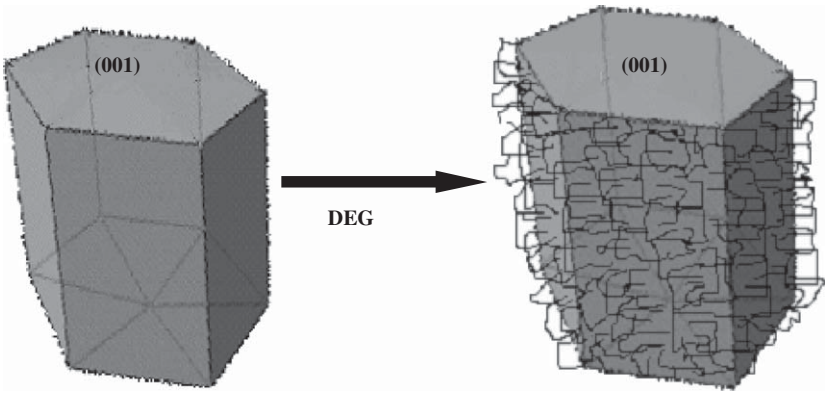

Fig. 6. A schematic view of showing the primary particles of ZnO with the DEG molecules adsorbed on its non-polar faces.

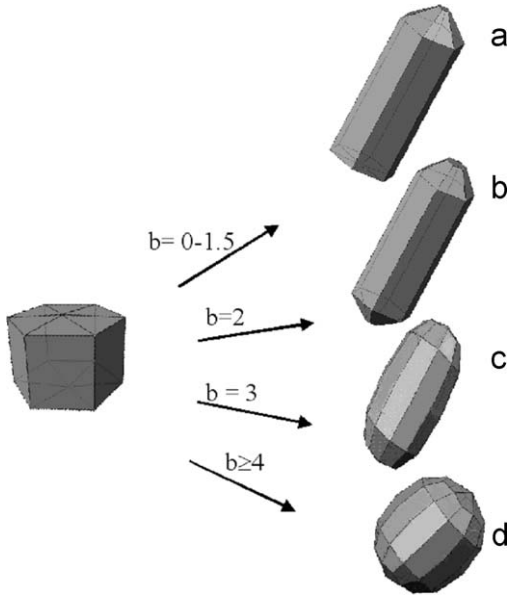

Fig. 8. Evolution of the ZnO particles morphology as a function of the alkaline ratio.

alkoxyacetate complexes: $Zn_3(OAc)_4(O(CH_2)_2O(CH_2)_2O)$ and $Zn_2(OAc)_3(OCH_2CH_2OH)$.

(ii) In a second step, the forced hydrolysis of the alcoxyacetate complex, accentuated by the increase of the OH^- concentration, leads to a partial substitution of the alcoxy anions, less electronegative than the acetate anions, by OH^- ions leading to an hydroxy-alkoxyacetate complex $[Zn(OAc)_{2-x}(O(CH_2)_2O(CH_2)_2O)_{x-y}(OH)_{2y}]$.

(iii) Finally, when elevating the temperature, the condensation of the hydroxy-alkoxyacetate complex, which may be concomitant with the hydrolysis reaction, leads to the progressive development of the ZnO nuclei and then the ZnO crystallites via olation and oxalation reactions.

This mechanism is very close to that generally occurring in the well known sol–gel process [26]. The main difference is that in the case of sol–gel process the alkoxyacetate is formed by the addition of acetic acid to an alcohol solution containing the alkoxide $M(OR)_n$ whereas here the alcoxyacetate is formed in situ starting from a zinc salt namely zinc acetate dissolved in polyol medium.

In conclusion, the difference observed in the morphology of the ZnO elaborated particles as a function of the concentration of OH^- ions could be interpreted from a kinetic point of view as follows: when the concentration is low, the hydrolysis of the alkoxyacetate complex proceeds slowly and also the condensation and the nucleation reactions. Progressive growth units will be formed and incorporated in the crystal lattice at the (0 0 1) interface resulting in conical and then in nanorod-like particles. For a large concentration, the formation of the hydroxy-alkoxyacetate complex was rapid and also the reactions of condensation and nucleation; the formation of all ZnO nuclei occurs almost at the same time resulting in particles with a spherical aspect. In our case, the presence of OH^- ions accelerates the pre-cited reactions (hydrolysis, condensation and nucleation), which could explain that with our synthesis conditions we elaborated ZnO particles even at 100 °C, while nucleation does not occur till the temperature reaches 150 °C in the synthesis conditions adopted by Lee et al. [16]. Finally, when using sodium acetate instead of hydroxide sodium, the rod-like morphology could be the result of the weak hydrolyzing ability of the $CH_3CO_2^-$ ions. In fact, in this case the bringing of the OH^- ions to the reaction medium will be progressive, so the hydrolysis process of the alkoxyacetate complex proceeds very slowly resulting in the observed elongated microscopic morphology.

3.5. Thermal analysis

The thermal decomposition behavior of the ZnO powders was examined by thermo-gravimetric analysis (TGA) between room temperature and 773 K. The result presented in Fig. 9 for the Zn_{28} powder, shows a total weight loss of about 1.4% between 373 and 750 K. The first gradual weight loss of about 0.5%, observed between 373 and 450 K, could be ascribed to the departure of residual water molecules adsorbed on the surface of the nanoparticles. The second gradient appearing between 450 and 750 K could be attributed to the progressive degradation of the polyol molecules adsorbed on the surface of the particles. These TGA measures show that the solvent molecules could not be entirely removed by ordinary washing procedures. This result has been already observed in our previous analysis of cobalt fibers [27] and also confirmed by other authors [28]. The presence of water and polyol molecules on the surface of the elaborated particles is also supported by the FT-IR study (Fig. 7) showing the bands corresponding to the bending and stretching vibrations of CH_2 of the polyol appearing, respectively, in the 1300–1650 and 2800–3000 cm^{-1} regions, the bands around 1650, 2325 and 2350 cm^{-1} corresponding to the bending mode of the OH groups of water and solvent and finally the broad bands around 3400 cm^{-1} corresponding to the stretching mode of the O–H groups [29,30].

3.6. Optical properties

3.6.1. The UV–vis absorption

Room-temperature UV–vis absorption spectra of the as-prepared ZnO particles are shown in Fig. 10. A strong UV absorption is characteristic of all measured samples, which attains a plateau above 3.3 eV (375 nm). The determination of the bandgap energy from these measurements is rather difficult because of the evident and strong Urbah's tail. However, a rough estimation can be obtained from the square-root absorbance extrapolation as suggested for the direct transitions $E_g \approx 3.25 \pm 0.05$ eV, which is in agreement with that of the bulk ZnO solids. This behavior is expected because the observed

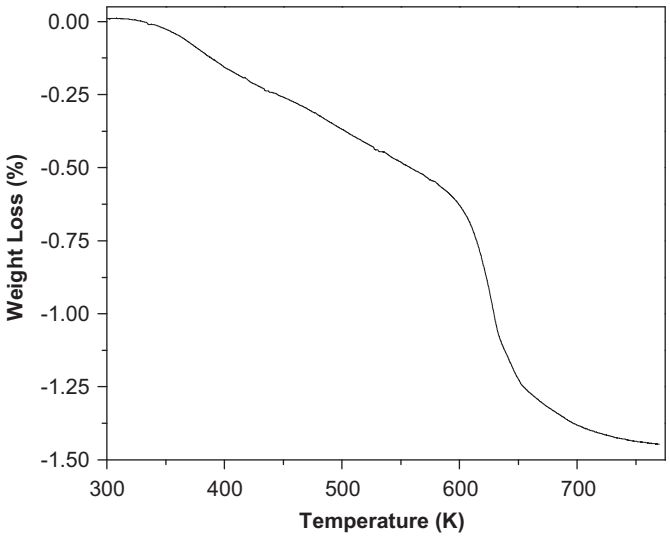

Fig. 9. TG curve of the conical particles from RT to 773 K.

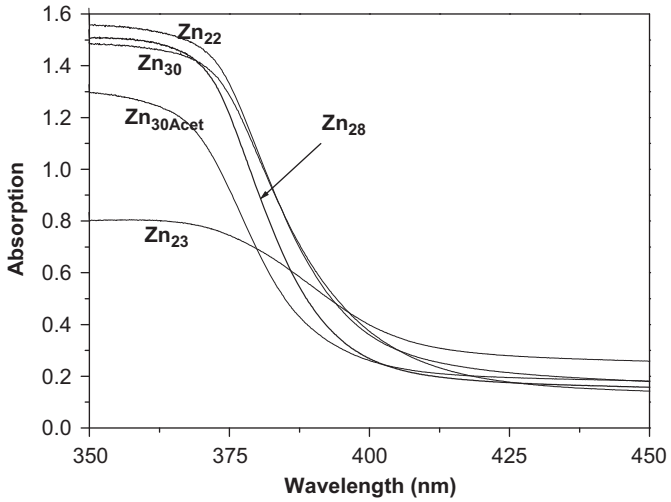

Fig. 10. UV–vis absorption spectra of ZnO particles with different morphologies: nanorods (sample Zn_{22}), irregular morphology (sample Zn_{23}), conical morphology (sample Zn_{28}), spherical morphology (sample Zn_{30}) and rod-like morphology (sample Zn_{30acet}).

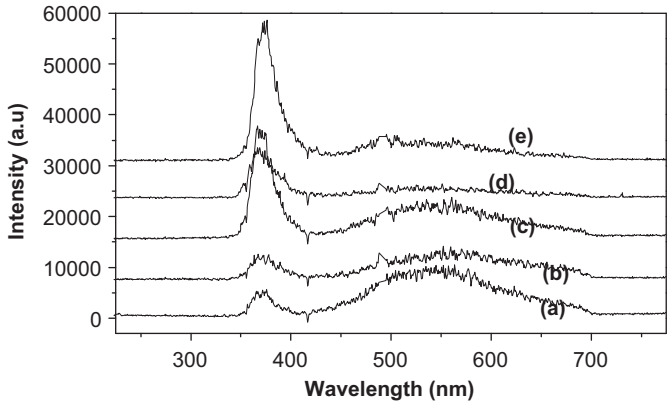

Fig. 11. Room-temperature photoluminescence (PL) spectra of ZnO particles presenting different morphologies: nanorods (a), spherical morphology (b), conical morphology (c), irregular morphology (d) and rod-like morphology (e).

particles are much larger than the ZnO exciton Bohr diameter of 2.5 nm [31]. More instructive seems to be inspecting the sub-band gap absorption, which weakens in order

$$Zn_{23} \rightarrow Zn_{22} \approx Zn_{30} \rightarrow Zn_{28} \rightarrow Zn_{30Acet} \quad (1)$$

This sequence may reflect the crystalline quality of the prepared samples.

3.6.2. Photoluminescence

Room-temperature photoluminescence spectra of the ZnO samples of different morphologies according to Table 1 (cone, nanorods, spheres, rods) are shown in Fig. 11. All samples exhibited a typical ZnO UV-excitonic emission band around 380 nm and the broad green band at 550 nm. For the visible green emission, at present there are several hypotheses about its origin including zinc vacancy (V_{Zn}), oxygen vacancy (V_O), oxygen interstitial (O_i) and antisite oxygen (O_{Zn}) [32,33]. Due to their small size, these particles have a very large surface-to-volume ratio, which may produce a large number of oxygen vacancies. We, therefore, believe that in our case the green emission is essentially due to surface single-ionised oxygen vacancies [34].

With some precaution related to the defect levels saturation, the intensity ratio of the UV to visible bands can be a measure of the sample quality; in fact, stronger is the visible band less stoichiometric is the sample. The measured intensity ratio of these bands in the ultraviolet and visible regions is given in Table 2; it increases in order

$$Zn_{22} \rightarrow Zn_{30} \rightarrow Zn_{28} \rightarrow Zn_{23} \rightarrow Zn_{30Acet} \quad (2)$$

According to Table 1, this ratio depends on the sample morphology and/or size. The lowest intensity ratio is then observed for the nanorods (sample Zn_{22}). The green band intensity weakens for the particles with spherical morphology (sample Zn_{30}) and then for the particles with conical morphology (sample Zn_{28}). These three samples (synthesized in identical experimental conditions with only one varied parameter-basic ratio) reasonably fit both relations (1) and (2), respectively, obtained from the absorption and PL measurements. The green emission band is practically absent in Zn_{30Acet} sample prepared with sodium acetate trihydrate, which can be apparently included in sequences (1) and (2).

Sequences (1) and (2) may be put in relation with the particles morphology and/or size. The most straightforward is to compare the surface-to-volume ratio (S/V) of particles obtained in similar elaboration conditions. In fact, for spherical particles of radius R (sample Zn_{30}) $S/V = 3/R$, while for cylindrical-shape particles of radius R and length L (samples Zn_{22} and M_{28}) $S/V = 2(R^{-1}+L^{-1})$. This sets a sequence in decreasing order of S/V

$$Zn_{30} \rightarrow Zn_{23} \rightarrow Zn_{22} \rightarrow Zn_{28} \approx Zn_{30Acet} \quad (3)$$

Though, the general tendency of (1) and (2) is maintained by (3) (we observe at the extremities samples Zn_{22}/Zn_{30} and Zn_{28}/Zn_{30Acet}) the quantitative correlation falls. Except for Zn_{23} that does not fit the sequences, the samples Zn_{22} and Zn_{30} exchange places. This indicates that their surface state changes. Apparently, the stretched morphology of sample Zn_{22} favors the creation of surface defects and excitons quenching.

The green emission band also vanishes in Zn_{23} sample, which, however, falls out of the above-considered relations. However, its comparison with Zn_{22}, Zn_{30} and Zn_{28} samples is not possible because of the different solvents used for its synthesis, ethylene glycol instead of diethylene glycol as well as the lower temperature. This modification may strongly affect the surface state and therefore relation (2). Since the elliptical-shape particles of sample Zn_{23} have similar surface-to-volume ratio to that of spherical particles of sample Zn_{30}, the observed difference in the band intensities cannot be assigned to this factor. We believe that the surface defects are critical to the temperature at which the sample is prepared; sample Zn_{30} elaborated at higher temperature (245 °C) compared to sample Zn_{23} (198 °C) results in a higher concentration of surface defects.

4. Conclusion

In conclusion, nanoparticles of ZnO with a diversity of morphologies (conical, nanorod-like, spherical, rod-like) have been prepared using the polyol process. These particles have good crystallinity, good dispersity and do not show macroscopic agglomeration. Their growth mechanism has been proposed on the basis of the zincite growth habit and the observation of the variation of morphology of the elaborated particles as a function of the synthesis condition, specially the concentration of OH^- ions added in the solution. TGA analysis proved that the solvent molecules could not be entirely removed by the ordinary wash

procedures. Photoluminescence measurements evidence excitonic UV and defect emission bands. The green band is assigned to surface oxygen vacancies of ZnO particles. The complimentary absorption and PL measurements allow concluding about the particle crystalline quality and surface state. In particular, by using the polyol process without any additional surface treatment and by adjusting synthesis parameters we succeeded in preparation of ZnO rods almost free of surface defects and impurities.

Acknowledgements

We thank Dr. A. Seguatni for his assistance while preparing the manuscript. A. Dakhlaoui is grateful to the IDB (Islamic Development BANK) for the financial support.

References

[1] Z. Deng, M. Chen, G. Gu, L. Wu, J. Phys. Chem. B 112 (2008) 16.
[2] S.J. Yang, Ch.R. Park, Nanotechnology 19 (2008) 035609.
[3] T. Krishnakumar, R. Jayaprakash, N. Pinna, V.N. Singh, B.R. Mehta, A.R. Phani, Mater. Lett. 63 (2) (2008) 242.
[4] B. Cao, W. Cai, J. Phys. Chem. C 112 (2008) 680.
[5] M. Li, H. Bala, X. Lv, X. Ma, F. Sun, L. Tang, Z. Wang, Mater. Lett. 61 (2007) 690.
[6] C.-F. Jin, X. Yuan, W.-W. Ge, J.-M. Hong, X.-Q. Xin, Nanotechnology 14 (6) (2003) 667.
[7] H. Udono, Y. Sumi, S. Yamada, I. Kikuma, J. Cryst. Growth 310 (2008) 1827.
[8] T. Tsuzuki, P.G. McCormick, Scr. Mater. 44 (2001) 1731.
[9] Y. Dai, Y. Zhang, Q.K. Li, C.W. Nan, Chem. Phys. Lett. 358 (2002) 83.
[10] Ch.-L. Zhang, W.-N. Zhou, Y. Hang, Z. Lü, H.-D. Hou, Y.-B. Zuo, S.-J. Qin, F.-H. Lu, S.-L. Gu, J. Cryst. Growth 310 (2008) 1819.
[11] S.E. Ahn, J.S. Lee, H. Kim, S. Kim, B.H. Kang, K.H. Kim, G.T. Kim, Appl. Phys. Lett. 84 (24) (2004) 5022.
[12] I.R. Collins, S.E. Taylor, J. Mater. Chem. 2 (1992) 1277.
[13] D. Jézéquel, J. Guenot, N. Jouini, F. Fiévet, J. Mater. Res. 10 (1995) 77.
[14] L. Poul, S. Ammar, N. Jouini, F. Fiévet, F. Villain, Solid State Sci. 3 (2001) 31.
[15] L. Poul, S. Ammar, N. Jouini, F. Fievet, F. Villain, J. Sol–Gel Sci. Technol. 26 (2003) 261.
[16] S. Lee, S. Jeong, D. Kim, S. Hwang, M. Jeon, J. Moon, Superlattices Microstruct. 43 (2008) 330.
[17] Z. Yang, Q. Liu, H. Yu, B. Zou, Y. Wang, T.H. Wang, Nanotechnology 19 (2008) 035704 (and references therein).
[18] X. Meng, D. Zhao, D. Shen, J. Zhang, B. Li, X. Wang, X. Fan, J. Lumin. 122–123 (2007) 766.
[19] P. Singjai, T. Jintakosol, S. Singkarat, S. Choopun, Mater. Sci. Eng. B 137 (2007) 59.
[20] Ch. Yan, D. Xue, J. Cryst. Growth 310 (2008) 1836.
[21] Ch. Wu, X. Qiao, J. Chen, H. Wang, F. Tan, S. Li, Mater. Lett. 60 (2006) 1828.
[22] B.G. Wang, E.W. Shi, W.Z. Zhong, Cryst. Res. Technol. 32 (1997) 659.
[23] L. Poul, Ph.D-Thesis, University Pierre-Marie Curie, Paris, France, 2000.
[24] L. Poul, N. Jouini, F. Fiévet, P. Herson, Z. kristallogr. 213 (1998) 416.
[25] Y. Wang, X. Jiang, Y. Xia, J. Am. Chem. Soc. 125 (2003) 16176 (and references therein).
[26] C. Sanchez, J. Livage, New J. Chem. 14 (1990) 513.
[27] A. Dakhlaoui, L.S. Smiri, G. Babadjian, F. Schoenstein, P. Molinie, N. Jouini, J. Phys. Chem. C 112 (2008) 14348.
[28] X.M. Liu, Y.C. Zhou, J. Cryst. Growth 270 (2004) 527.
[29] M. López-Sánchez, A. Domínguez-Vidal, M.J. Ayora-Cañada, A. Molina-Díaz, Anal. Chim. ACTA 620 (2008) 113.
[30] T.K.K. Srinivasan, C.I. Jose, A.B. Biswas, Can. J. Chem. 47 (1969) 3877.
[31] S. Monticone, R. Tufeu, A.V. Kanaev, J. Phys. Chem. B 102 (1998) 2854.
[32] M.K. Patra, K. Manzoor, M. Manoth, S.R. Vadera, N. Kumar, J. Lumin. 128 (2008) 267.
[33] T. Sun, J. Qiu, Ch. Liang, J. Phys. Chem. C 112 (2008) 715.
[34] S. Yamamoto, H. Yano, T. Mishina, J. Nakahara, J. Lumin. 126 (2007) 257.